An Internal-Variable Constitutive Model for Semisolid Slurries At High Solid Fractions

O.J. Ilegbusi and M.D. Mat

(Submitted 31 July 1997; in revised form 2 October 1997)

A mathematical model is proposed to represent the thixotropic behavior of semisolid slurries at high solid fractions (f_s > 0.6), as occurs in dispersion-strengthened metal-matrix composite processing. The model assumes that the slurry behaves as a viscoplastic porous medium saturated with liquid phase and hardened or softened, depending on the shear rate and solid fraction. The model is validated by comparison of its predictions with a recent set of experimental data on Sn-Pb alloys.

Keywords rheology, slurries, Sn-Pb alloys

1. Introduction

Processing of materials in the semisolid state has become a potentially attractive means of producing near-net parts from segregation-prone alloys and controlling the microstructure. It involves partially solidifying a melt or partially melting a solid to produce solid particles in a liquid matrix. The solid fraction may vary over a wide range, depending on the application, and the microstructure can be dendritic as in conventional solidification or globular as a consequence of vigorous stirring during the solidification. The stirred slush becomes thixotropic and its viscosity decreases with the stirring speed and time.

Although semisolid processing has existed as a net-shape forming technology for many years, the flow behavior of semisolid metal alloys is still poorly characterized at high solid fractions. This is the subject of the present investigation.

The constitutive behavior of semisolid alloys is very complex, as it depends on the solid fraction, the morphology of the solid phase, and the thermochemical history. As a result, most previous works on the constitutive behavior of semisolid slurries have been limited to low solid fractions. In that range, the solid particles are not fully connected and the slurry rheology is history-dependent. However, the flow resistance increases dramatically as the solid fraction reaches a critical value representing the development of an interconnected network, and it is highly dependent on the particle morphology and the degree of agglomeration between the particles.

The constitutive behavior of semisolid slurries has been widely studied. Brown (Ref 1) introduced an internal variable or structural variable to represent the degree of agglomeration among the solid particles, fluid phase viscosity, particle size morphology, and distribution of particle sizes. The extensive set of experimental data of Joly and Mehrabian (Ref 2) with rounded particles showed that the flow resistance after some transient period would continue to decrease with increase in shear stress due to the breaking of the particle agglomerates. Kattamis et al. (Ref 3) used a Coutte-type viscometer to demonstrate that increasing the cooling rate results in smaller particle size and higher apparent viscosity for a given solid fraction.

The kinetics of agglomeration and disagglomeration of the primary phase particles in semisolid Al-6Si alloy reinforced with SiC particles was studied by Mada and Ajerch (Ref 4). An analytical model was developed based on the analogy of dissociation and restructuring with chemical reaction.

Several models have been proposed to represent slurry viscosity at high solid fractions (Ref 5-9). Most of these models consider the slurry as a viscoplastic porous medium saturated with a liquid phase and impose a power-law dependence of the strain rate on shear stress. Thus, a constant slurry viscosity is predicted after the flow field becomes fully developed. However, such a trend contradicts recent experimental evidence (Ref 9) that the slurry exhibits thixotropic (history-dependent) behavior even at high solid fractions. Therefore, the objective of the present study was to develop a constitutive model that accounts for this thixotropy at high solid fractions. The model was based on the internal-variable concept of Brown (Ref 1), with a modification for the high solid loading. It was assumed that thixotropy occurs due to the structural change under shear.

2. Formulation

Consider two concentric cylindrical vessels simulating a Couette rheometer (Fig. 1). The slurry consisting of Sn-15wt%Pb alloy is contained in the annulus, while the outer cylinder is rotated

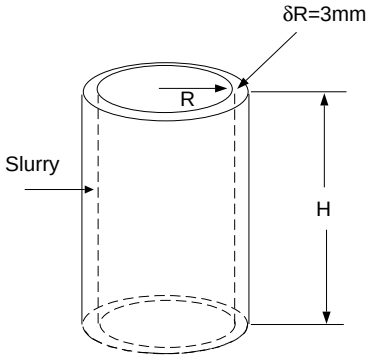

Fig. 1 Schematic sketch of the problem considered

O.J. Ilegbusi and **M.D. Mat,** Department of Mechanical, Industrial and Manufacturing Engineering, Northeastern University, Boston, MA 02115, USA.

around the stationary inner cylinder to provide a shear force. This system mirrors the experimental setup of Martin et al. (Ref 9) to afford direct comparison of the numerical results with the experimental data. The principal input parameters used in the computation are presented in Table 1.

This problem may be stated mathematically in terms of the axial, radial, and azimuthal components of the equation of motion, together with that for mass conservation. Assuming cylindrical symmetry, the governing equations can be expressed as Mass conservation:

$$\frac{\partial w}{\partial t} + \frac{1}{r}\frac{\partial rw}{\partial r} = 0 \qquad \text{(Eq 1)}$$

Axial momentum:

$$\rho \frac{\partial}{\partial t}(w) + \rho\nabla \cdot (\mathbf{u}w) = -\frac{\partial p}{\partial z} - (\nabla \cdot \tau)_z \qquad \text{(Eq 2)}$$

Radial momentum:

$$\rho \frac{\partial}{\partial t}(v) + \rho\nabla \cdot (\mathbf{u}v) = -\frac{\partial p}{\partial r} - (\nabla \cdot \tau)_r \qquad \text{(Eq 3)}$$

Azimuthal momentum:

$$\rho\frac{\partial}{\partial t}(u) + \rho\nabla \cdot (\mathbf{u}u) = -(\nabla \cdot \tau)_\theta \qquad \text{(Eq 4)}$$

where $\mathbf{u}$ is the velocity vector, u is the viscosity, ρ is the density, p is the pressure, τ is the shear stress tensor, and u, v, and w are the azimuthal, radial, and axial components of the velocity vector, respectively, in the cylindrical coordinate system.

2.1 Constitutive Relationship

The parameter τ in Eq 2 to 4 is the shear stress tensor through which the constitutive relationship is represented. In general, the stress components can be expressed in terms of the slurry apparent viscosity, μ, and the shear rates, γ, in tensorial notation as (Ref 10):

$$\tau_{ij} = -\mu\left(\frac{\partial U_i}{\partial x_j} + \frac{\partial U_j}{\partial x_i}\right) \qquad \text{(Eq 5)}$$

Table 1 Principal input data used in the computations

Parameter	Value
Height of cylinder (H), m	0.06
Outer radius of cylinder (R_{out}), m	0.023
Inner radius of cylinder (R), m	0.02
Density of slurry (ρ), kg/m^3	8107
Reference viscosity of slurry (μ), Pa · s	0.04

where subscripts i and j refer to the coordinate directions and U and x represent the generalized velocity and spatial coordinates, respectively. For example, the $\tau_{r\theta}$ component of the shear stress is:

$$\tau_{r\theta} = -\mu\left[r\frac{\partial}{\partial r}\left(\frac{u}{r}\right) + \frac{1}{r}\frac{\partial v}{\partial \theta}\right] \qquad \text{(Eq 6)}$$

Most of the existing models of slurry viscosity at high solid fractions assume a viscoplastic medium saturated with liquid. Thus, the flow resistance is principally due to the thermally activated plastic deformation of welds between the solid particles, and a power-law dependence of the strain rate on shear stress is usually assumed (Ref 5-9). A useful relationship can be derived for slurry viscosity from the recent work of Martin et al. (Ref 9) thus:

$$\mu = 2\gamma^{(1-m)/m}\alpha^{-1}\beta^{-1/m}A(f_s)^{-(1+m)/2m}\exp\left(\frac{-Q}{RT}\right)^{-1/m} \qquad \text{(Eq 7)}$$

where γ is the shear rate, f_s is the fraction of solid in the slurry, α and β are empirical constants that depend on the material, Q is the activation energy required for visco-plastic solid deformation, R is the universal gas constant, T is the temperature, m is the power law exponent with a value of 5.7 established experimentally by Nguyen et al. (Ref 5) for Sn-15wt%Pb alloys, and $A(f_s)$ is a function of the solid fraction and shape of the solid. Martin et al. (Ref 9) proposed the following functional relationship for globular microstructure:

$$A(f_s) = \frac{3.0}{f_s^{1.5}} \qquad \text{(Eq 8)}$$

While Eq 7 may provide a basis for representing slurry behavior, it has a major drawback in that the shear stress calculated with it is invariant with the shear rate at constant temperature and solid fraction. Such trend contradicts the recent experimental result of Martin et al. (Ref 9) in which the slurry exhibits thixotropic behavior even at high solid fractions. To adequately represent such behavior, it is assumed here that the microstructure continues to evolve even at high solid loading and that thixotropy results from this structural evolution. In analogy to the work of Brown (Ref 1) at low solid fractions, we propose adding a thixotropic term to Eq 7 of the form:

$$\mu_{th} = S(\gamma, f_s)\gamma^{(m-1)/m} \qquad \text{(Eq 9)}$$

such that the effective viscosity μ_{eff} at high solid loading is:

$$\mu_{eff} = \mu + \mu_{th} \qquad \text{(Eq 10)}$$

In Eq 9, $S(\gamma, t)$ is an internal variable that represents the structural evolution. Evidence for the form of $S(\gamma, t)$ may be provided by the limited data of Martin et al. (Ref 9) at high solid

fraction in which there occurs an initial exponential shear stress/shear strain dependence and a subsequent decay of the shear stress with strain after a threshold strain. The data also suggest that this critical strain may be dependent on the shear rate. While additional data will be needed to confirm these conclusions, we propose the following functional relationship for S:

$$S(\gamma, t) = H(\gamma) \exp(-ct) \quad \text{(Eq 11)}$$

where $H(\gamma)$ is a shear-rate-dependent function and c is a parameter used to express the agglomeration and disagglomeration of particles, depending on the shear rate relative to the critical value γ_{crit}. This parameter may be expressed as:

$$c = d(\gamma_{crit} - \gamma) \quad \text{(Eq 12)}$$

where d is an empirical coefficient to be determined by systematic comparison of predictions with the experimental data (described in the following section).

Equations 11 and 12 in effect imply that if $\gamma < \gamma_{crit}$, the slurry continues to agglomerate while disagglomeration occurs thereafter. The disagglomeration of the slurry after a critical strain, as observed by Martin et al. (Ref 9), can be accommodated by making the coefficient d strain dependent. It can also be deduced from the data of Martin et al. (Ref 9) that γ_{crit} is a power-law function of the solid fraction. This functional relationship is here represented as:

$$\gamma_{crit} = e f_s^m \quad \text{(Eq 13)}$$

where m is the power-law exponent and e is an empirical constant, both to be determined by systematic comparison of predictions with the experimental data. The values of the model constants based on the limited experimental data are given in Table 2.

2.2 Boundary Conditions

A zero-slip condition is imposed on the velocity components on all the solid surfaces. The fluxes of all variables are neglected at the free surface.

3. Solution Procedure

The governing equations are solved with a modified version of the PHOENICS computational package (Ref 11), for which a new routine was added to represent the non-Newtonian slurry behavior. The velocities are first calculated from a Newtonian fluid formulation to obtain a preliminary deformation tensor. Next, the viscosity is calculated using the formulation proposed in Eq 10. The transport equations are then solved with

Table 2 Values of model constants used in the computations

Constant	Value
α, MPa^{-1}	0.03
β	4.5
d, s	0.1
e, s^{-1}	140.0
m	5.7
Q, kJ/kg	257
R, kJ/kg · K	8.13

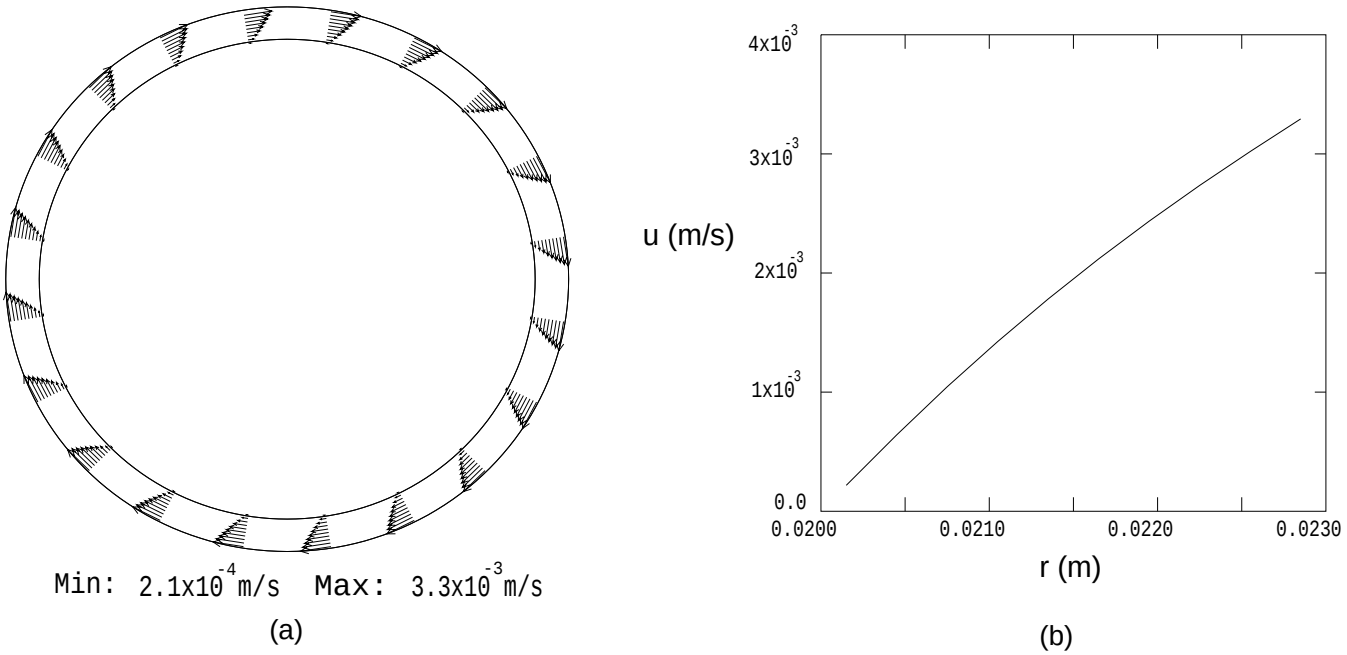

Fig. 2 Velocity profile (a) and radial variation of the velocity (b) at $z = H/2$ for $\gamma = 0.1\ s^{-1}$

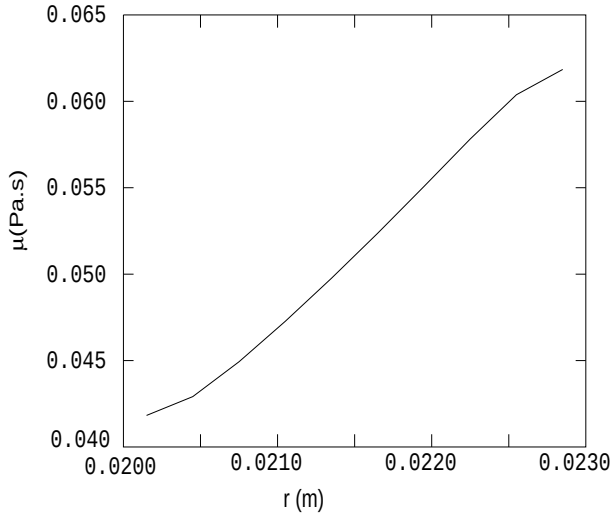

Fig. 3 Radial variation of viscosity at $z = H/2$ for $\gamma = 0.1\ s^{-1}$ and $f_s = 0.63$

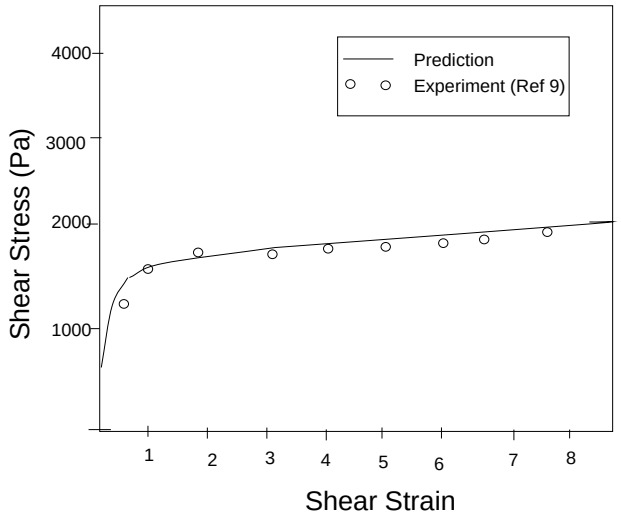

Fig. 4 Stress-strain curve for $\gamma = 0.1\ s^{-1}$ and $f_s = 0.63$

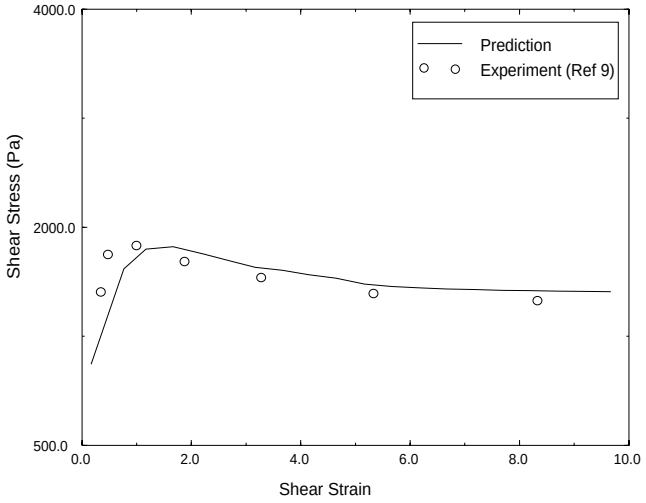

Fig. 5 Stress-strain curve for $\gamma = 1.0\ s^{-1}$ and $f_s = 0.63$

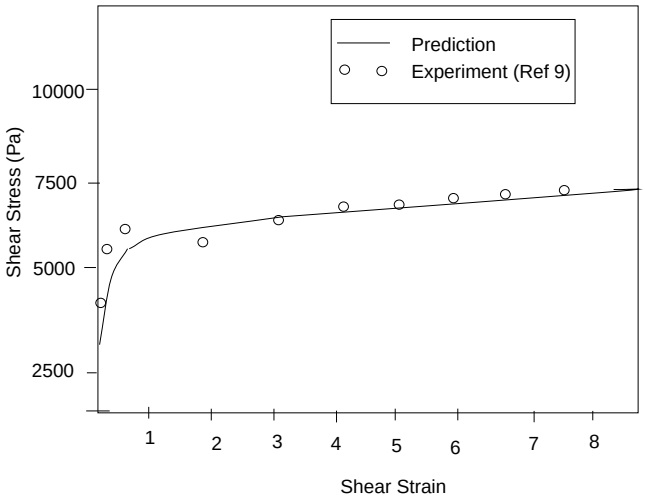

Fig. 6 Stress-strain curve for $\gamma = 1.0\ s^{-1}$ and $f_s = 0.7$

the new viscosity at the same time step until the solution converges. The numerical procedure uses an implicit finite-domain formulation of the equations and the SIMPLER algorithm (Ref 12). The results are verified for numerical accuracy through systematic refinement of the temporal and spatial grids until the results become grid independent. Typically, 15 by 20 by 20 grids in the r, θ, and z directions and 0.01 time step are required for grid independence.

4. Results

Figure 2(a) shows the velocity profile at mid-height for a shear rate $\gamma = 0.1\ s^{-1}$ after a shear strain of 5. The corresponding radial variation of velocity at $z = H/2$ is presented in Fig. 2(b). The distribution is essentially laminar, as evidenced by the approximately linear variation in velocity between the cylinders. This result may be associated with the assumed no-slip conditions at the walls. While this assumption may not be valid at high solid loading due to slippage, the present result may be considered adequate because slippage can be minimized in a real situation by putting grooves on the rheometer walls.

Figure 3 shows the variation of the viscosity of the slurry along the radial direction at $z = H/2$. The non-Newtonian behavior is quite evident as the viscosity decreases toward the stationary inner cylinder ($r = 0.02$ m) where the shear stress is highest.

Figure 4 compares the predicted shear stress-strain relation with the experimental data of Martin et al. (Ref 9) for a Sn-15Pb alloy with $\gamma = 0.1\ s^{-1}$ and $f_s = 0.63$. The agreement between the predictions and measurement is quite good over the entire range. The shear stress increases with the shear strain. The variation is initially rapid until a strain of about 1.0 and stress of 1800 Pa, and it subsequently approaches a steady

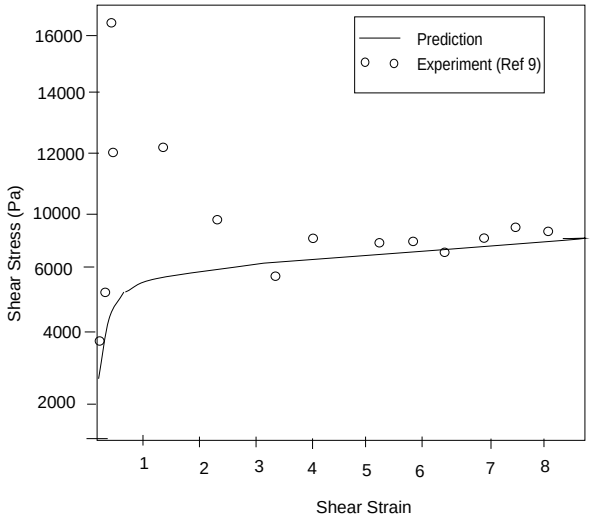

Fig. 7 Stress-strain curve for $\gamma = 10.0\ s^{-1}$ and $f_s = 0.7$

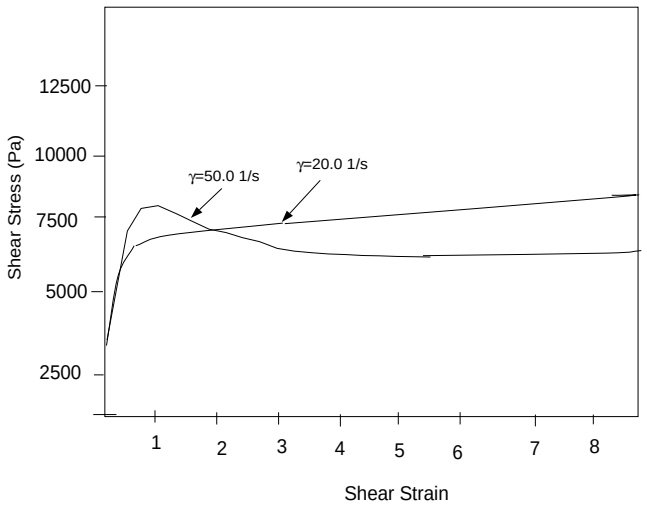

Fig. 8 Stress-strain curve for $f_s = 0.8$ and $\gamma = 20.0\ s^{-1}$, $\gamma = 50\ s^{-}$

state. This result provides strong support for the exponential term in the proposed model Eq 11.

Figure 5 shows the shear stress response of the slurry at a higher shear rate ($\gamma = 1.0\ s^{-1}$). Again, the experimental data of Martin et al. (Ref 9) are adequately represented by the proposed model. The shear stress initially increases until a critical shear strain is reached, after which it decreases.

Figures 6 and 7 show the shear stress-strain relation at a higher solid fraction, $f_s = 0.7$. Figure 6 compares the prediction and the experimental data for $\gamma = 1\ s^{-1}$ and Fig. 7 compares the results at $\gamma = 10.0\ s^{-1}$. The shear stress in both cases continuously increases with the shear strain. Because the shear stress does not decay at any stage of the strain, the results suggest that for this high solid fraction the critical shear stress may be higher than that observed in Fig. 4 and 5 for a lower solid fraction, $f_s = 0.63$. The large discrepancy between the predicted shear stress and the experimental data at low strains in Fig. 7 may be due to other physical mechanisms in play at that range, such as a positive shear sensitivity of the materials at high solid fractions (Ref 13).

The calculations were carried beyond the experimental information to predict the slurry behavior at an even higher solid fraction and higher shear rates. Typical results are presented in Fig. 8 for $\gamma = 20.0\ s^{-1}$ and $\gamma = 50\ s^{-1}$ for $f_s = 0.8$. Although such high solid loading may be difficult to achieve in practice, the results are quite instructive. There is indeed a breakdown of the structure at high shear rates, even for very high solid loading, as evidenced by the subsequent decrease in the shear stress after a critical maximum value.

5. Conclusions

A mathematical model is presented to represent the rheological behavior of semisolid slurries at high solid fractions. The model is based on the internal-variable concept in which thixotropy is associated with the structural change of the slurries under shear. The main proposal is that the slurry behavior at high solid fractions exhibits a shear decay with strain after a critical shear stress that depends on the solid fraction. This decay may be attributed to the deformation of liquid welds under shear.

The model predictions agree quite well with the available experimental data for Sn-15wt%Pb alloy at solid fractions of 0.63 and 0.7. The model is also applied beyond the available experimental data for a system at a higher solid fraction of 0.8 and higher shear rates of $20s^{-1}$ and $50s^{-1}$. The shear stress/shear strain curve exhibits a continuously exponential behavior at low shear rates and low-to-moderate solid fractions. The stress decays after a critical shear stress for higher solid fractions. Additional experimental data are needed to further develop and validate the model. Such data will provide evidence for relating the model constants to the spatial and temporal distribution of the solid morphology.

The mathematical model developed here can provide guidance in specifying stable and acceptable processing paths for semisolid materials. The model also can be applied to other solid/liquid systems that exhibit thixotropic behavior in net-shape processing. Such systems include ceramic/polymer carrier systems and particulate- and short-fiber-reinforced metal-matrix composites. Furthermore, the model is ideally suited for studying mold filling and fractionation of semisolid slurries.

Acknowledgment

The financial support of the National Science Foundation under grant DMI-9612497is gratefully acknowledged.

References

1. S.B. Brown, An Internal Variable Constitute Model for the Thixotropic Behavior of Metal Semi-Solid Slurries, *Proc. ASM/TMS Fall Conference*, 1989
2. P.A. Joly and R. Mehrabian, The Rheology of a Partially Solid Alloy, *J. Mater. Sci.*, Vol 11, 1976, p 1393-1418
3. T.Z. Kattamis and T.J. Piccone, Rheology of Semi-Solid Al-4.5%Cu-1.5%Mg Alloy, *Mater. Sci. Eng.*, Vol A131, 1991, p 265-272

4. M. Mada and F. Ajerch, Thixotropic Effects in Semi-Solid Al-6%Si Alloy Reinforced with SiC Particles, *Metal and Ceramic Matrix Composites: Processing, Modeling and Mechanical Behavior*, The Minerals, Metals and Materials Society, 1990, p 337-350
5. T.G. Nguyen, M. Suery, and D. Favier, Mechanical Behavior of Semi-Solid Alloys under Drained Compression with Lateral Pressure, *Proc. Second Int. Conf. Processing of Semi-Solid Alloys and Composites*, S.B. Brown and M.C. Flemings, Ed., MIT, 1992, p 296-304
6. J.S. Gunasekera, Development of a Constitutive Model for Mushy (Semi-Solid) Materials, *Proc. Second Int. Conf. Processing of Semi-Solid Alloys and Composites*, 1992, p 211-222
7. S.P. Wang and K.K. Wang, Die Casting of Semi-Solid Metals, *Proc. 2nd Int. Conf. Processing of Semi-Solid Alloys and Composites*, 1992, p 336-345
8. P.V. Hernandez, A.M. Chaze, and C. Levaillant, Rheological Behavior of Zn-Sn Alloy in the Solidification Range, *Proc. Second Int. Conf. Processing of Semi-Solid Alloys and Composites*, S.B. Brown and M.C. Flemings Ed., MIT, 1992, p 316-327
9. C.L. Martin, S.B. Brown, D. Favier, and M. Suery, Shear Deformation of High Solid Fraction (>0.60) Semi-Solid Sn-Pb under Various Structures, *Mater. Sci. Eng.*, Vol A202, 1995, p 111-122
10. O.J. Ilegbusi, Application of a Time-Dependent Constitutive Model to Rheocast Systems, *JMEPEG*, Vol 5, 1996, p 117-123
11. H. Rosten and D.B. Spalding, "*PHOENICS Beginner's Guide and User's Manual*," Technical Report 100, CHAM Limited, 1986
12. S.V. Patankar and D.B. Spalding, A Calculation Procedure for Heat, Mass and Momentum Transfer in Three-Dimensional Parabolic Flows, *Int. J. Heat Mass Trans.*, Vol 15, 1972, p 1787-1806
13. A.R.A. McLelland, N.G. Henderson, H.V. Atkinson, and C.M. Sellars, Semi-Solid Processing and Microstructure in MMCs Based on Hypereutectic Al/Si Alloys, *Proc. Second Int. Conf. Processing of Semi-Solid Alloys and Composites*, S.B. Brown and M.C. Flemings Ed., MIT, 1992, p 290-295